SCIENCE CHINA Life Sciences

Dogs lacking Apolipoprotein E show advanced atherosclerosis leading to apparent clinical complications

Zhao Hui[1], Zhao Jianping[2], Di Wu Di[3], Sun Zhaolin[2], Hua Yang[4], Zheng Min[2], Liu Yumei[5], Yang Qi[6], Huang Xiahe[7], Li Yuan[2], Piao Yueshan[4], Wang Yingchun[8], Lam Sin Man[9], Xu Huijuan[10], Shui Guanghou[11], Wang Yongjun[12], Yao Haifeng[13], Lai Liangxue[14], Du Zhuo[15], Mi Jidong[16], Liu Enqi[17], Ji Xunming[18] and Zhang Yong Q.[19]

Citation: SCIENCE CHINA Life Sciences (2021); doi: 10.1007/s11427-021-2006-y

View online: https://engine.scichina.com/doi/10.1007/s11427-021-2006-y

Published by the Science China Press

Dogs lacking Apolipoprotein E show advanced atherosclerosis leading to apparent clinical complications

Hui Zhao[1,2†], Jianping Zhao[3†], Di Wu[4†], Zhaolin Sun[3†], Yang Hua[4], Min Zheng[3], Yumei Liu[4], Qi Yang[4], Xiahe Huang[1], Yuan Li[3], Yueshan Piao[4], Yingchun Wang[1], Sin Man Lam[1], Huijuan Xu[1], Guanghou Shui[1], Yongjun Wang[5], Haifeng Yao[6], Liangxue Lai[2], Zhuo Du[1], Jidong Mi[3]*, Enqi Liu[7]*, Xunming Ji[4]* & Yong Q. Zhang[1]*

[1]Key Laboratory of Molecular Developmental Biology, and CAS Center for Excellence in Brain Science and Intelligence Technology, Institute of Genetics and Developmental Biology, Chinese Academy of Sciences, Beijing 100101, China;

[2]Guangzhou Institutes of Biomedicine and Health, Chinese Academy of Sciences, Guangzhou 510530, China;

[3]Beijing Sinogene Biotechnology Co. Ltd, Beijing 102200, China;

[4]Xuanwu Hospital, Capital Medical University, Beijing 100053, China;

[5]TianTan Hospital, Capital Medical University, Beijing 100070, China;

[6]Beijing Petsguard Animal Hospital, Beijing 100192, China;

[7]Laboratory Animal Center, Xi'an Jiaotong University Health Science Center, Xi'an 710049, China

*Corresponding authors (Yong Q. Zhang, email: yqzhang@genetics.ac.cn; Jidong Mi, email: mijidong@163.com; Enqi Liu, email: liuenqi@mail.xjtu.edu.cn; Xunming Ji, email: 7)

†Contributed equally to this work

Received July 5, 2021; accepted August 31, 2021

ABSTRACT

Atherosclerotic cardiovascular disease resulting from dysregulated lipid metabolism is the leading cause of morbidity and mortality worldwide. Apolipoprotein E (ApoE) plays a critical role in cholesterol metabolism. Knockouts in lipid-metabolizing proteins including ApoE in multiple model organisms such as mice and rats exhibiting elevated levels of cholesterol have been widely used for dissecting the pathology of atherosclerosis, but few of these animal models exhibit advanced atherosclerotic plaques leading to ischemia-induced clinical symptoms, limiting their use for translational studies. Here we report hypercholesterolemia and severe atherosclerosis characterized by stenosis and occlusion of arteries, together with clinical manifestations of stroke and gangrene, in *ApoE* knockout dogs generated by CRISPR/Cas9 and cloned by somatic cell nuclear transfer technologies. Importantly, the hypercholesterolemia and atherosclerotic complications in F0 mutants are recapitulated in their offspring. As the ApoE-associated atherosclerosis and clinical manifestations in mutant dogs are more similar to that in human patients compared with those in other animal models, these mutant dogs will be invaluable in developing and evaluating new therapies, including endovascular procedures, against atherosclerosis and related disorders.

Key words: ApoE, atherosclerosis, hypercholesterolemia, gangrene, stroke

INTRODUCTION

Atherosclerosis, a progressive inflammatory disease characterized by accumulation of lipids in, and hence thickening of, the arterial walls, is the leading cause of death worldwide (Libby et al., 2011). Hypercholesterolemia correlates directly with the extent and progression of atherosclerosis (Goldstein et al., 2015). Mouse model with apolipoprotein E (*ApoE*) mutated has been the most widely used model of atherosclerosis, which develops severe hypercholesterolemia and fibroatheromatous atherosclerosis on a regular diet (Plump et al., 1992). However, there are limitations of the mouse model for atherosclerosis including the rarity of plaque ruptures and superimposed thrombosis, and the lack of advanced atherosclerosis in the coronary, carotid and cerebral arteries leading to clinical consequences (Libby et al., 2011; Bentzon and Falk, 2010). Thus, large animal models showing similar artery size and cerebrovascular anatomy as the humans are required for developing therapies of endovascular procedures which have become the main treatment options for atherosclerotic patients (Herrmann et al., 2019).

ApoE plays a key role in cholesterol metabolism (Mahley, 1988). A key physiological role of ApoE is its ability to mediate high-affinity binding of ApoE-containing lipoproteins to the low-density lipoprotein (LDL) receptor, resulting in the uptake and degradation of lipoproteins and the use of lipoprotein cholesterol. Loss of ApoE protein in human plasma results in familial type III hyperlipoproteinemia, characterized by accumulations of very low-density lipoprotein (VLDL), intermediate-density lipoprotein (IDL), and chylomicron remnants and a higher risk of atherosclerotic disease (Ghiselli et al., 1981; Mahley et al., 1999). Genetic studies have revealed that variants in *ApoE* are associated with the susceptibility to coronary heart disease and stroke (Bennet et al., 2007; Khan et al., 2013). *ApoE* knockout (KO) mice, rats, rabbits, and pigs show increased levels of cholesterols together with apparent atherosclerosis in large arteries such as the aorta (Zhang et al., 1992; Plump

et al., 1992; Shim et al., 2017; Fang et al., 2018; Niimi et al., 2016; Zhao et al., 2018). However, clinical manifestations associated with advanced atherosclerosis have been rarely reported in these *ApoE* mutants.

Domestic dogs (*Canis lupus familiaris*) are an ideal model for studying human diseases due to their close similarities to humans in anatomy and physiology (Tsai et al., 2007; Feng et al., 2018). Moreover, due to the cohabitation and co-evolution of dogs with humans for more than 30,000 years, they share similar diets and daily life patterns, leading to similar patterns of non-communicable diseases to those found in humans (Wang et al., 2013; Ostrander et al., 2017; 2019). To provide an alternative model for atherosclerosis, we previously generated an *ApoE* KO mutant dog by CRISPR/Cas9, followed by cloning with somatic cell nuclear transfer technologies (Feng et al., 2018). Here we report that these animals were fully fertile and did not show any apparent medical concerns before the age of 18 month adults (dogs are sexually mature at 12 months). However, all four F0 *ApoE* KO dogs, together with their mutant offspring, developed severe and widespread atherosclerosis leading to complications including gangrene and ischemic stroke at the age of 18–24 month old, faithfully mimicking the pathology in human patients of advanced atherosclerosis.

RESULTS

ApoE KO dogs develop stroke or gangrene

In a previous study, we generated an *ApoE* KO dog we named Apple by CRISPR/Cas9 editing, from which other three mutant dogs were cloned by somatic cell nuclear transfer (Feng et al., 2018) (the 4 mutants are thereafter referred to as mutants 1–4, respectively). All four dogs exhibited hypercholesterolemia at one month old (Feng et al., 2018) and appeared normal and fertile without any discernable anomalies when fed on a regular diet until 18 months old. Here we report that *ApoE* KO dogs developed severe

advanced atherosclerosis accompanied by clinical complications at 19–24-month old, an age equivalent to about 40 years of human beings (Wang et al., 2020). *ApoE* mutant 1 at 24 months old could not stand and lay on the right side and appeared to suffer a stroke. Magnetic Resonance Imaging (MRI) of the brain of the mutant 1 by T2-weighted (T2W) and fluid attenuated inversion recovery (FLAIR) procedures showed a large ischemic infarct of 7.41 cm^3 covering the frontal, parietal, and temporal lobes in the left hemisphere (Figure 1, A and B), consistent with right-sided paralysis. In addition, there was a second smaller, acute infarction of 1.14 cm^3 detected by diffusion weighted imaging (DWI) and apparent diffusion coefficient (ADC) imaging in the left basal ganglia due to a relatively recent event (< 3 days after stroke) (Figure 1, C and D). The large infarct in the brain of mutant 1 was consistent with the results of postmortem examination (Figure 1, E) when the animal was sacrificed 20 days after the initial stroke and paralysis. Similar MRI analyses of the other three 18-month-old mutants (mutants 2, 3 and 4 cloned from mutant 1) did not show evidence of infarction in the brain. Stroke did not occur in all mutants, probably because collateral circulation exists in the blood vessels of the basal part of the dog brain (Figure 1, F-H).

However, all three cloned mutants (mutants 2 to 4) developed gangrene at 19 months old in their distal parts of the rear limbs (Figure 1, I and J), likely due to atherosclerotic stenosis of the femoral arteries (Table 1) which provide blood to rear limbs. Postmortem analysis of all four F0 mutant dogs also showed unevenly bulged and yellowish basilar artery (Figure 1, F-H) in the brain and coronary arteries (Figure 1, K-M) in the heart (all died before 24 months old), indicative of advanced atherosclerosis pathology.

We further analyzed F0 mutant 1 after stroke by electrocardiography (ECG) and found signs of myocardial ischemia evidenced by S-T depression and T-wave deep inversion (Figure S1A). The myocardial creatinine kinase (CK, 391 u/L in mutant while the normal range is 10-200 u/L) and lactate

Severe atherosclerosis in *ApoE* KO dogs by histological examination

To understand the pathology associated with *ApoE* mutations in dogs, we examined the blood vessels for signs of atherosclerosis by histological analysis. Consistent with the ultrasonography analysis, postmortem analysis showed compelling evidence of advanced atherosclerosis in the basilar, coronary, internal carotid, and femoral arteries of ApoE-deficient dogs (Figure 1 and Table 1). We stained arteries with H&E, Masson's trichrome stain (labeling muscle fibers in red and collagen fibers in blue), antibodies against smooth muscle actin (SMA) and macrophage marker CD68 (Figure 3, A-D). WT control dogs (n = 4) showed no lesions in all arteries examined by ultrasonography and postmortem analysis. The structure of an artery wall consists of tunica intima, tunica media, and tunica adventitia separated by internal and external elastic lamina, respectively (Figure 4). Histological examination of arteries further showed advanced atherosclerosis in the basilar artery, coronary artery, internal carotid artery, and femoral artery of *ApoE* KO dogs (Figures 3, A–E and 4, A–I, and Figure S2). The advanced atherosclerosis led to severe stenosis and occlusion of basilar artery, coronary artery, as well as femoral artery and internal carotid artery, but other large arteries such as common carotid, abdominal and thoracic aorta showed normal vascular lumen (Figure 3, E). Immunostaining with an antibody against CD68, a pan-macrophage marker, revealed infiltration of macrophages to all layers of blood vessel and adjacent myocardium (Figure 3). The severity and distribution of atherosclerotic lesions in the arteries of the *ApoE* mutants were consistent with a previous report on high fat diet-induced atherosclerosis and thrombosis in dogs (Mahley et al., 1976). Importantly, the basilar arteries, coronary arteries, internal carotids, and femoral arteries, the most affected in *ApoE* mutant dogs (Figures 3, 4, Figure S2, and Table 1), are frequently affected in human atherosclerosis patients (Stary et al., 1995; Bentzon et al., 2014).

F2 homozygous *ApoE* KO dogs recapitulate the hypercholesterolemia and atherosclerosis of F0 mutants

To determine if atherosclerosis observed in F0 mutants can be transmitted to the next generation via germ line, we bred the cloned F0 mutants 2 and 3 (to avoid possible mosaics and off-targeting in the founder mutant 1) for two generations and obtained homozygous F2 *ApoE* KO dogs. Re-examination of the genotypes of F1 and F2 offspring showed that the original *ApoE* mutations in F0 founder mutants were -34+17 bp (NC_006583.4 range 110006660..110009463 complement, g.1484_1517delinsCCTGGACCAGGGAGGCT) as previously reported in one allele (Feng et al., 2018) and -2236 bp (g.237_2471del) in another, resulting in early termination of the protein (XP_533644, p.Leu38ProfsTer26) and deletion of all coding exons, respectively. The heterozygous F1 dogs carrying -34+17 or -2236 bp transmitted the mutant alleles in a Mendelian fashion, producing the expected number of F2 dogs (WT: heterozygous: homozygous = 6: 12: 8).

Similar to our observation in *ApoE* F0 mutants, we detected atherosclerosis by ultrasonography in four viable F2 *ApoE* homozygous KOs of 9 to 17 months old (the genotype of one mutant is -2236/-2236 bp, while the genotype of the remaining three is -34+17/-34+17 bp). Apparent plaque or stenosis was found in the carotid, abdominal aorta, and femoral arteries of one 17 months old F2 *ApoE* KO (Table 2). The other three F2 *ApoE* KO dogs (-34+17/-34+17 bp) at 9, 12, and 17 months old also showed thickened intima-media in femoral arteries and carotid arteries by ultrasonography, while all the WT (n = 13) dogs examined showed no sign of atherosclerosis (Table 2). The earliest stage at which we observed atherosclerosis by ultrasonography was 9 months of the homozygous -34+17/-34+17 bp mutant (Table 2).

One F2 homozygous *ApoE* mutant dog (-2236 bp/-2236 bp) developed gangrene at 18 months old in distal parts of the two rear limbs. Postmortem

analysis of the mutant (sacrificed due to severe gangrene) showed bulged and yellowish coronary arteries with apparent atherosclerosis in the coronary artery and occlusion of femoral artery (Figure S2).

To analyze apolipoprotein changes in the mutants, we performed sodium dodecyl sulfate-polyacrylamide gel electrophoresis (SDS-PAGE) analysis of the plasma fractionations by sequential ultracentrifugation and found that the apolipoprotein profiles in WT dogs were similar to what is reported for rabbits (Niimi et al., 2016; Niimi et al., 2021). We further found no ApoE protein but a marked increase of ApoB-48 in the VLDL and IDL fractions, along with increased ApoA1 and ApoA4 in the VLDL fraction of the homozygous F2 mutants (Figure 5A).

We examined the plasma from F0, F2 and F3 mutants for alterations in triglyceride (TG) and cholesterol levels. As with *ApoE* mutant patients (Ghiselli et al., 1981) and pigs (Shim et al., 2017 and Fang et al., 2018) on a regular diet, we observed normal TG levels in all mutants examined (Tables 3, 4), consistent with a normal TG level in F0 mutants before weaning in our previous report (Feng et al., 2018). However, a significantly elevated level of total cholesterol (TC) was observed in all four F0 *ApoE*

mutants (Tables 3, 4). In summary, the hypercholesterolemia in *ApoE* mutants was recapitulated in the homozygous F2 and F3 mutant progeny (Tables 3, 4).

The lipid composition of the plasma of all four F0 *ApoE* mutant dogs was further analyzed by lipidomic profiling. We found that the levels of major lipid components such as cholesterols but not medium-chain triacylglycerols and phosphatidic acids were significantly up-regulatedr (Figure 5B), confirming hypercholesterolemia and normal TG levels in *ApoE* KO mutants.

We also examined other atherosclerosis related factors such as blood pressure and inflammation in mutants. The blood pressure in mutant dogs at age of 6–21 months showed no difference from WT controls (systolic pressure = 122.5±3.7 mmHg in WT controls and 110.5±2.9 mmHg in mutants, diastolic pressure = 70.2±4.1 mmHg in WT controls and 69.0±12 mmHg in mutants; n = 11 for WT controls, n = 4 for F2 mutants). Plasma level of the C reactive protein (CRP) serves as an indicator of inflammation. Our analysis of plasma showed that the CRP was significantly elevated in F2 KO mutants at 11–17 month old (less than 5 mg/L in WT controls and 25.58 2.74 mg/L in KO mutants, n = 3 in each genotype). The increase in the level of CRP, together with the infiltration of CD68-positive macrophages in arteries of mutants (Figure 3), supports the notion that atherosclerosis is closely associated with inflammation.

Proteomic analysis reveal altered lipid metabolism and inflammation in *ApoE* KO dogs.

How does loss of ApoE lead to altered lipid metabolism and atherosclerosis? To get a global overview of the molecular pathways regulated by ApoE, we performed high-throughput mass spectrometry to identify protein expression alterations in the plasma of all four F0 *ApoE* mutants and the liver of mutant 1. In the plasma, we detected 331 proteins, 55 (17%) of which showed differential expressions in mutants (49 upregulated and six

downregulated; Figure 6A and Supplemental Table 1). More widespread protein expression changes were observed in the liver of mutant 1, where 57% (1,688 out of 2,955 proteins) of proteins were differentially expressed (Figure 6B and Supplemental Table 1). As expected, ApoE protein levels were dramatically reduced in both plasma and the liver of *ApoE* mutants (Figure 6, A–C). Further SDS-PAGE of plasma fractionations by sequential ultracentrifugation detected no ApoE protein in the mutants (Figure 5A), consistent with the molecular nature of the frameshift mutation at the 38th Leu. Other apolipoprotein family members were up-regulated (ApoA4 and ApoB etc.) or down-regulated (e.g., ApoA1) in the plasma as a direct or indirect result of ApoE loss (Figure 6C). Increased ApoB and ApoB/ApoA1 ratio were proposed to predict cardiovascular events in humans (Sierra-Johnson et al., 2009).

Functional enrichment analysis of upregulated proteins revealed that six processes were co-enriched in both plasma and liver, including blood microparticles, complement and coagulation cascades, extracellular space, and extracellular exosomes (Figure 6, D and E, and Supplemental Table 2), while many other biological processes showed distinct enrichment patterns between the two samples of plasma and liver. For example, proteins related to LDL particles and membrane attack complexes were enriched in the plasma, whereas proteins involved in acute-phase response and the positive regulation of heterotypic cell-cell adhesion were enriched in the liver (Figure 6, D and E).

To further evaluate the role of *ApoE* in human diseases such as stroke, we determined whether these differentially expressed proteins overlapped with stroke related proteins and genome-wide association study (GWAS)-positive stroke gene products. We interrogated the proteome of plasma and liver with a list of 446 human stroke related genes compiled from public databases and literature using an array of key words (see materials and methods) (Supplemental Table 3) and identified 438 canine homologs. Of which, 41 were

expressed in the plasma. Eight out of 41 were upregulated while one was downregulated in the plasma of *ApoE* mutants. Of the 438 canine homologs, 112 were expressed in the liver. Among the 112 homologs, 26 were upregulated and 55 were downregulated in the liver of *ApoE* mutant 1. These canine homologs were significantly over-represented (>1.7-fold enrichment) in up- but not down-regulated proteins in the liver of *ApoE* mutant 1 (Figure 6F and Supplemental Table 1). Out of 47 GWAS-positive stroke genes reported so far (Supplemental Table 4), there are 44 canine homologs. There were four out of 44 homologs identified in the plasma proteome, none of the four was dysregulated in *ApoE* mutants. However, seven out of eight canine homologs of GWAS-positive genes for stroke showed significant protein level changes of up (FGA, CD163 and CRP) or down (ANK2, CDC5L, WNK1 and SYNE2) in the liver of *ApoE* mutant 1 (Figure 6G and Supplemental Tables 4 and 5). FGA is the alpha subunit of the coagulation factor fibrinogen, which is a component of blood clot. CD163 is exclusively expressed in monocytes and macrophages. The significantly increased levels of CD163 and CRP indicate inflammation in mutants. These results, particularly of liver proteomics analysis, provided experimental support for a critical role of *ApoE* and its associated pathways in stroke etiology.

DISCUSSION

Though dogs show different lipoprotein profiles such as relative HDL/LDL levels from humans (Yin et al., 2012), dogs lacking *ApoE* show an elevated LDL-C/HDL-C ratios (Tables 3, 4) as in human patients and provide invaluable addition to the commonly used mouse models for the study of atherosclerosis and its associated complications with distinct advantages. First, advanced atherosclerosis characterized by plaque rupture and near occlusion of basilar and coronary arteries was observed in *ApoE* mutant dogs, similar to that in human atherosclerosis patients (Stary et al., 1995; Bentzon et al., 2014), but

has been rarely documented in other animal models. Prominent atherosclerosis mostly occurs in the proximal aorta of mice and rabbits (Zhang et al., 1992; Plump et al., 1992; Niimi et al., 2016), whereas the most important clinical consequences of atherosclerosis in humans arise from lesions in the coronary, carotid and cerebral arteries (Libby et al., 2011; Stary et al., 1995; Bentzon et al., 2014) which were fully recapitulated in the adult *ApoE* mutant dogs. The apparent differences in severity and site of atherosclerosis between *ApoE* mutant mice and dogs could be due to differences in blood flow dynamics, vessel anatomy and elaboration, ageing, the duration under hypercholesterolemia, or a combination of any of the five factors. The upregulated CD163 and CRP in the mutants from proteomic analysis indicates inflammation facilitating atherosclerosis, while the upregulated complement and coagulation cascades in the mutants promote blood clotting increasing the risk of stroke or gangrene.

We note that individual mutants show variations in phenotypes; the F0 mutant 1 exhibits the strongest phenotype of atherosclerosis while the homozygous -34+17 bp F2 mutant shows the weakest (Figure 1 and Tables 1, 2). The variation in the severity of atherosclerosis correlates positively with LDL-C levels (for LDL-C levels in individual F0 mutants, see Feng et al., 2018) and may be caused by different genotype (-34+17/-2236 bp in F0 and -2236/-2236 bp or -34+17/-34+17 bp in F2), genetic background (Beagle dogs are not a pure inbred line), environment (all three cloned F0 mutants were mothered by different bitches; different batches of feed), or a combination of any of the three factors. Hypertension is an independent risk factor for stroke. However, we found a normal blood pressure in F2 mutants, consistent with normal blood pressures in *ApoE* KO mice (Trieu and Uckun, 1998; Weiss et al., 2001). We suspect that the stroke in mutant 1 was mainly, if not fully, caused by severe atherosclerosis resulting from hypercholesterolemia. We predict that the F2 *ApoE* mutants will likely to develop gangrene with aging rather than

stroke because of the severe atherosclerosis in femoral arteries, while stroke needs confounding secondary factors such as a ruptured plaque and thrombus nearby blocking blood supply to the brain.

Second, atherosclerosis and its associated stroke in dog models can be readily examined using hospital-based non-invasive ultrasound analysis and MRI, respectively, facilitating evaluation of disease progression and prognosis. Third, endovascular operations are the main treatment options for atherosclerotic patients (Herrmann et al., 2019). The large size of arteries and severe atherosclerotic pathologies in *ApoE* dogs make them an attractive model for developing novel endovascular treatments. Finally, we used cloned *ApoE* mutants which can be obtained in large numbers with high efficiency for pathological analysis, so that functional analysis can be achieved in identical genetic background with minimum individual variance. Mutant dogs have been bred into a large colony in a relatively short period of time due to the rapid reproduction cycle (12 months to be sexually mature, three pregnancies per two years and about six progeny per pregnancy). Thus, we envisage that the *ApoE* KO dogs we generated can be used to develop effective therapies such as stents and flow diverters for ischemic attack in the brain and heart, as the larger size of arteries and the advanced atherosclerosis in dogs are better suited for surgical intervention than that in the small rodent models. In summary, although dog models are limited to some extent by a high cost and ethical controversy, the *ApoE* KO dogs will be valuable for developing new drugs and interventional strategies for atherosclerosis and associated complications.

MATERIALs and METHODSs

Animals.

We previously generated one male *ApoE* KO dog by CRISPR/Cas9 editing followed by cloning by somatic cell nuclear transfer technology (Feng et al., 2018). We considered all four mutants, mutant 1 and its cloned progeny 2, 3, and 4, strong hypomorphs or nulls as they carried no ApoE expression by proteomic analysis.

Naturally weaned Beagles were housed individually in pens (180 × 90 × 90 cm) and exposed to a 12: 12 light-dark cycle (lights on at 0600 h). They were fed at 0900 h and 1700 h with a regular commercial dog diet (28% crude protein, 9.5% fat, 6.2% crude ash, 1.55% calcium, and 1.84% phosphorus; Bomei, Xingtai, China). All experiments were approved by the Animal Care and Use Committee of Beijing Sinogene Biotechnology Co., Ltd (No.XNG-IAC-201801).

Biochemical analysis of plasma lipoproteins

Lipid and lipoprotein analysis of the plasma was performed on F0 mutant dogs (n = 4) and WT controls (n = 10) at 18~24 months. Blood samples were taken from the limb venous plexus into EDTA (ethylene diamine tetraacetic acid) anticoagulant tubes. The levels of total cholesterol, triglycerides, HDL cholesterol and LDL cholesterol were determined by routine protocols at Dian Diagnostics (Nanjing, China). We performed SDS-PAGE of fractionated plasma after sequential ultracentrifugation following a previously reported protocol (Niimi et al., 2021). C reactive protein level (CRP), the myocardial creatinine kinase (CK) and lactate dehydrogenase (LDH) were determined using Catalyst One (IDEXX, USA). Blood pressure was measured using CONTEC08A-VET (CONTEC, Japan).

MRI analysis and ultrasound examination

All MRI images were acquired on a 3T whole body scanner (Tim Verio, Siemens Healthcare, Erlangen, Germany) with a 32 channel head coil following published protocols for the canine brain (Packer et al., 2018). Imaging modes included T2 weighted (T2W), fluid attenuated inversion recovery (FLAIR), diffusion weighted imaging (DWI), and apparent diffusion coefficient (ADC) imaging. MRI images were processed with OsiriX MD (version 9.0.1) (Federau et al., 2016). Infarct volumes were calculated using ITK-Snap contouring software (Pittsburgh) with stacks of average diffusion images reconstructed in three dimensions

The ultrasound scan of large blood arteries of adult dogs was performed following a previously published protocol (Grant et al., 2003) using Ascendus (HITACHI-ALOKA) with broadband linear transducers (3.0–7.0 MHz) or a convex array probe (4.0–8.0 MHz). Control and *ApoE* mutant dogs of 1.5–2 years old were sedated by propofol at 8–12 mg/kg. The carotid and peripheral arteries including bilateral carotid artery, femoral artery and abdominal aorta were examined by regular procedures. First, the two-dimensional gray-scale mode (B mode) was used to examine artery lumen and wall structures including lumen diameter, intima-media thickness, and the distribution and extent of plaques. Second, the color Doppler flow imaging was applied to examine the filling of blood. Last, the spectral Doppler mode was used to measure the blood flow velocity including peak systolic velocity (PSV) and end diastolic velocity (EDV) in carotid arteries. The severity of atherosclerosis from weak to strong is thickened (intima-media thickness), plaque, stenosis, and occlusion. Based on the general practice in patients (Grant et al., 2003; Stein et al., 2008), we define “thickened” as abnormally increased intima-media thickness by less than 50%, “plaque” as defined by an increase of greater thickness by more than 50% than the surrounding intima-media thickness, “stenosis” as vascular lumen diameter less than 50% compared with normal diameter, and “occlusion” as almost no blood flow.

We performed electrocardiography to *ApoE* mutant 1 after stroke using an electrocardiograph (ECG-3C, Aricon, China) by default parameters.

Histological analysis of arteries

For immunostaining, the arteries of *ApoE* mutant (n = 4 in F0 and 1 in F2) and WT control dogs (n = 4) were removed and fixed for 48 hours in 4% paraformaldehyde (PFA) prepared in 1× PBS (Na_2HPO_4 8 mM, NaCl 136 mM, KH_2PO_4 2 mM, KCl 2.6 mM). PFA-fixed artery segments were embedded in paraffin, and 4-μm sections were stained with hematoxylin and eosin and Masson's trichrome. Adjacent sections were stained with antibodies against smooth muscle α-actin (SMA; ZM-0003, Zhongshanjinqiao) to reveal vascular smooth muscle cells, and CD68 (ZM-0060, Zhongshanjinqiao) to stain macrophages. All staining images were acquired with a Nikon Eclipse Ci microscope. Lesions in the cross-section of arteries were traced manually using ImageJ. The percentage of increased intimal area (pathologies from plaques to occlusions) filling up the vascular lumen (area delineated by elastic fiber) was statistically calculated by ImageJ.

Proteomic analysis of plasma and liver

Protein preparation for mass spectrometric analysis

The plasma of individual dogs (4 control dogs and 4 F0 mutant dogs) was treated (1:1) with 4% sodium dodecyl sulfate (SDS) in 0.1 M Tris-HCl, pH 7.6. Three adjacent pieces of liver tissues from one control and one mutant dog (mutant dog 1) were individually lysed in a buffer (5 times volume of 150 mg tissue weight) consisting of 0.05 M Tris-HCl, pH 7.4, 0.15 M NaCl, 1% Triton X-100, 1% sodium deoxycholate, and 1% SDS at 99 °C for 10 min. The protein concentrations were determined using a BCA protein assay kit (Thermo Scientific, Rockford, IL).

Protein Digestion and TMT Labeling

Protein digestion was performed using the filter-aided proteome preparation (FASP) method. Briefly, protein was reduced by 100 mM DTT at 37°C for 1 hour, and the reduced proteins were transferred into the Microcon YM-30 centrifugal filter units (EMD Millipore Corporation, Billerica, MA) to allow buffer exchange. After exchanged to the UA buffer (8 M urea, 100mM Tris-HCl, pH 8.5), the protein was alkylated by 55 mM iodoacetamide (IAA, Sigma-Aldrich, Saint Louis, MO) for 1 hour in the dark. A buffer containing 0.1 M triethylammonium bicarbonate (TEAB, Sigma-Aldrich, Saint Louis, MO) was used to replace the denaturing buffer of the sample. Proteins were then digested with sequencing grade trypsin (Promega, Madison, WI) at 37°C overnight, and the resultant tryptic peptides were labeled with acetonitrile-dissolved TMT reagents (Thermo Scientific, Rockford, IL) by incubation at room temperature in dark for 2 hours. The labeling reaction was stopped by 5% hydroxylamine, and an equal amount of labeled samples were mixed together before off-line prefractionation with reversed phase (RP)-high performance liquid chromatography (HPLC).

RP-HPLC

Pre-fractionation of protein samples was performed using an offline basic RP-HPLC approach. The peptides were fractionated on a phenomenex gemini-NX 5μ C18 column (250 x 3.0 mm, 110 Å) (Torrance, CA, USA) using a Waters e2695 separations HPLC system. A 97 min basic RP-LC gradient with a flow rate of 0.4 mL/min as previously described was used for the entire LC separation (Udeshi et al., 2013). The separated samples were collected and combined into 10 fractions. All samples were dried with a Speed-Vac concentrator and stored at -20°C before use.

LC-MS/MS/MS analysis

The LC-MS/MS/MS analysis was performed using an Orbitrap Fusion™ Lumos™ Tribrid™ mass spectrometer (ThermoFisher Scientific) coupled online to an Easy-nLC 1200 in the data-dependent mode. The dried peptides

were resuspended in 0.1% formic acid (FA), and about 1 μg of each sample was injected into a capillary analytic column (length: 25 cm, inner diameter: 150 μm) packed with C18 particles (diameter: 1.9 μm). The LC was run with mobile phases containing buffer A (0.1 % FA) and buffer B (80 % ACN, 0.1 % FA). A 120-min non-linear gradient with a flow rate of 600 nL/min was used for peptide separation. The positive ion mode was used for MS measurements, and the spectra were acquired across the mass range of 375–1500 m/z. For each cycle of 3 s duration, one full MS scan was acquired in the Orbitrap at a resolution of 120,000 with automatic gain control (AGC) target of 5 × 105. After a full scan, multiple peptide ions were selected for MS/MS scan, which was followed (for plasma samples) or not followed (for liver samples) by MS/MS/MS scan. For MS/MS scan, the peptide ions were fragmented by collision-induced dissociation (CID) and analyzed in the linear ion trap with an AGC target of 1 × 104. For MS/MS/MS scan, up to the 10 most intense ions from each MS/MS scan were selected for fragmentation in the HCD cell using an AGC of 1 × 105. The resultant fragment ions were detected in the Orbitrap at a resolution of 50,000 at m/z 200 (for plasma samples labeled with 10-plex TMT reagent) or 15,000 at m/z 200 (for liver samples labeled with 6-plex TMT reagent).

Differential expression and functional enrichment analysis

Raw protein levels were log10 transformed and scaled between 0 and 1. Protein expression was compared between wild type and ApoE deficient mutants by *t*-test and those with a Benjamini-Hochberg corrected $P < 0.05$ were defined as differentially expressed proteins. Functional enrichment analysis was performed using the DAVID Functional Annotation tool with default parameters. Significantly enriched terms (Gene Ontology terms and KEGG pathways) were defined as those with a Benjamini corrected *P* value < 0.05.

Mass spectrometry analysis of plasma lipids

Samples from plasma of individual F0 *ApoE* KO dogs and WT controls (n = 4 for each group) were analyzed in a single mass spectrometric run as previously described (Lam et al., 2018). Lipids were analyzed using an Exion UPLC system coupled with a triple quodrupole/ion trap mass spectrometer (QTRAP 6500 Plus, Sciex). Separation of individual lipid classes were conducted by normal phase HPLC using a Phenomenex Luna silica column (3 mm, 150×2.0 mm). Student's *t* test was used to compare the changes in lipid levels between the two groups.

Analysis of stroke related and GWAS-positive gene homologs in *ApoE* mutant dogs

From interrogation of public databases of OMIM (online mendelian inheritance in man), HPO (human phenotype ontology), HGMD (human gene mutation database), and PubMed with an array of key words, we compiled a list of 446 stroke related genes (Supplemental Table 3). The key words we used were hereditary diseases (including monogenic, mendelian, single-gene, disorder, disease), genetic mutations (including pathogenic mutation, base pair mismatch, DNA repeat expansion, trinucleotide repeat expansion, frameshift mutation, gain of function mutation, gene amplification, gene duplication, genomic instability, microsatellite instability, germ-line mutation, indel mutation, loss of function mutation, missense mutation, point mutation, deletion, inversion, and lethal mutation), and cerebrovascular disorders (including stroke, cerebrovascular disease, ischemic stroke, brain infarction, transient ischemic attack, intracerebral hemorrhage, subarachnoid hemorrhage, aneurysm, moyamoya disease, moyamoya syndrome, artery dissection, arterial-venous malformation, and systematic embolic). We identified 438 canine homologs of the 446 human stroke related genes. Of the canine homologs, 41 are expressed in the plasma and 112 were expressed in the

liver.

Out of 47 GWAS-positive stroke genes reported so far (Supplemental Table 4), there are 44 canine homologs. There were four out of 44 homologs identified in the plasma proteome, but none of the four was misregulated in *AopE* mutants. However, seven out of eight GWAS-positive stroke gene homologs identified in the liver were misregulated in the *ApoE* mutant 1.

Statistics

Statistical analyses were performed with GraphPad Prism 6.0 (www.graphpad.com). All data are presented as the mean ± SEM. *P* values were calculated using a 2-tailed student's *t* test when two groups were compared, while one-way ANOVA was used when multiple groups were compared. *$P < 0.05$; **$P < 0.01$; ***$P < 0.001$.

References

Bennet, A.M., Di Angelantonio, E., Ye, Z., Wensley, F., Dahlin, A., Ahlbom, A., Keavney, B., Collins, R., Wiman, B., de Faire, U., et al. (2007). Association of apolipoprotein E genotypes with lipid levels and coronary risk. Jama 298, 1300-1311.

Bentzon, J.F., Falk, E. (2010). Atherosclerotic lesions in mouse and man: is it the same disease? Curr Opin Lipidol 21, 434-440.

Bentzon, J.F., Otsuka, F., Virmani, R., Falk, E. (2014). Mechanisms of plaque formation and rupture. Circ Res 114, 1852-1866.

Fang, B., Ren, X., Wang, Y., Li, Z., Zhao, L., Zhang, M., Li, C., Zhang, Z., Chen, L., Li, X., et al. (2018). Apolipoprotein E deficiency accelerates atherosclerosis development in miniature pigs. Dis Model Mech 11, dmm036632.

Federau, C., Mlynash, M., Christensen, S., Zaharchuk, G., Cha, B., Lansberg, M.G., Wintermark, M., Albers, G.W. (2016). Evolution of Volume and Signal Intensity on Fluid-attenuated Inversion Recovery MR Images after Endovascular Stroke Therapy. Radiology 280, 184-192.

Feng, C., Wang, X., Shi, H., Yan, Q., Zheng, M., Li, J., Zhang, Q., Qin, Y., Zhong, Y., Mi, J., et al. (2018). Generation of ApoE deficient dogs via combination of embryo injection of CRISPR/Cas9 with somatic cell nuclear transfer. J Genet Genomics 45, 47-50.

Ghiselli, G., Schaefer, E.J., Gascon, P., Breser, H.B., Jr. (1981). Type III hyperlipoproteinemia associated with apolipoprotein E deficiency. Science 214, 1239-1241.

Goldstein, J.L., Brown, M.S. (2015). A century of cholesterol and coronaries: from plaques to genes to statins. Cell 161, 161-172.

Grant, E.G., Benson, C.B., Moneta, G.L., Alexandrov, A.V., Baker, J.D., Bluth, E.I., Carroll, B.A., Eliasziw, M., Gocke, J., Hertzberg, B.S., et al. (2003). Carotid artery stenosis: gray-scale and Doppler US diagnosis--Society

of Radiologists in Ultrasound Consensus Conference. Radiology 229, 340-346.

Herrmann, A.M., Meckel, S., Gounis, M.J., Kringe, L., Motschall, E., Mulling, C., Boltze, J. (2019). Large animals in neurointerventional research: A systematic review on models, techniques and their application in endovascular procedures for stroke, aneurysms and vascular malformations. J Cereb Blood Flow Metab 39, 375-394.

Khan, T.A., Shah, T., Prieto, D., Zhang, W., Price, J., Fowkes, G.R., Cooper, J., Talmud, P.J., Humphries, S.E., Sundstrom, J., et al. (2013). Apolipoprotein E genotype, cardiovascular biomarkers and risk of stroke: systematic review and meta-analysis of 14,015 stroke cases and pooled analysis of primary biomarker data from up to 60,883 individuals. Int J Epidemiol 42(2), 475-492.

Lam, S.M., Wang, R., Miao, H., Li, B., Shui, G. (2018). An integrated method for direct interrogation of sphingolipid homeostasis in the heart and brain tissues of mice through postnatal development up to reproductive senescence. Anal Chim Acta 1037, 152-158.

Libby, P., Ridker, P.M., Hansson, G.K. (2011). Progress and challenges in translating the biology of atherosclerosis. Nature 473, 317-325.

Mahley, R., Nelson, A.W., Ferrans, V.J., Fry, D.L. (1976). Thrombosis in association with atherosclerosis induced by dietary perturbations in dogs. Science 192, 1139-1141.

Mahley, R.W. (1988). Apolipoprotein E: cholesterol transport protein with expanding role in cell biology. Science 240, 622-630.

Mahley, R.W., Huang, Y., Rall, S.C. Jr. (1999). Pathogenesis of type III hyperlipoproteinemia (dysbetalipoproteinemia). Questions, quandaries, and paradoxes. J Lipid Res 40, 1933–1949.

Niimi, M., Yang, D., Kitajima, S., Ning, B., Wang, C., Li, S., Liu, E., Zhang, J., Eugene Chen, Y., Fan, J. (2016). ApoE knockout rabbits: A novel model

for the study of human hyperlipidemia. Atherosclerosis 245, 187-193.

Niimi, M., Yan, H., Chen, Y., Wang, Y., Fan, J. (2021) Isolation and analysis of plasma lipoproteins by ultracentrifugation. J Vis Exp 167, e61790.

Ostrander, E.A., Wayne, R.K., Freedman, A.H., Davis, B.W. (2017). Demographic history, selection and functional diversity of the canine genome. Nat Rev Genet 18, 705-720.

Ostrander, E.A., Wang, G.D., Larson, G., vonHoldt, B.M., Davis, B.W., Jagannathan, V., Hitte, C., Wayne, R.K., Zhang, Y.P.; Dog10K Consortium. (2019). Dog10K: an international sequencing effort to advance studies of canine domestication, phenotypes and health. Natl Sci Rev 6(4), 810-824.

Packer, R.A., Rossmeisl, J.H., Kent, M.S., Griffin, J.F.t., Mazcko, C., LeBlanc, A.K. (2018). Consensus recommendations on standardized magnetic resonance imaging protocols for multicenter canine brain tumor clinical trials. Vet Radiol Ultrasound 59, 261-271.

Plump, A.S., Smith, J.D., Hayek, T., Aalto-Setala, K., Walsh, A., Verstuyft, J.G., Rubin, E.M., Breslow, J.L. (1992). Severe hypercholesterolemia and atherosclerosis in apolipoprotein E-deficient mice created by homologous recombination in ES cells. Cell 71, 343-353.

Shim, J., Poulsen, C.B., Hagensen, M.K., Larsen, T., Heegaard, P.M.H., Christoffersen, C., Bolund, L., Schmidt, M., Liu, Y., Li, J., et al. (2017). Apolipoprotein E deficiency increases remnant lipoproteins and accelerates progressive atherosclerosis, but not xanthoma formation, in gene-modified minipigs. JACC Basic Transl Sci 2, 591-600.

Sierra-Johnson, J., Fisher, R.M., Romero-Corral, A., Somers, V.K., Lopez-Jimenez, F., Ohrvik, J., Walldius, G., Hellenius, M.L., Hamsten, A. (2009). Concentration of apolipoprotein B is comparable with the apolipoprotein B/apolipoprotein A-I ratio and better than routine clinical lipid measurements in predicting coronary heart disease mortality:

findings from a multi-ethnic US population. Eur Heart J 30, 710-717.

Stary, H.C., Chandler, A.B., Dinsmore, R.E., Fuster, V., Glagov, S., Insull, W., Jr., Rosenfeld, M.E., Schwartz, C.J., Wagner, W.D., Wissler, R.W. (1995). A definition of advanced types of atherosclerotic lesions and a histological classification of atherosclerosis. A report from the Committee on Vascular Lesions of the Council on Arteriosclerosis, American Heart Association. Circulation 92, 1355-1374.

Stein, J.H., Korcarz, C.E., Hurst, R.T., Lonn, E., Kendall, C.B., Mohler, E.R., Najjar, S.S., Rembold, C.M., Post, W.S., American Society of Echocardiography Carotid Intima-Media Thickness Task Force. (2008). Use of carotid ultrasound to identify subclinical vascular disease and evaluate cardiovascular disease risk: a consensus statement from the American society of echocardiography carotid intima-media thickness task force endorsed by the society for vascular medicine. J Am Soc Echocardiography 21, 93–111.

Trieu, V.N., Uckun, F.M. (1998). Male-associated hypertension in LDL-R deficient mice. Biochem Biophys Res Commun 247(2), 277-279.

Tsai, K.L., Clark, L.A., Murphy, K.E. (2007). Understanding hereditary diseases using the dog and human as companion model systems. Mamm Genome 18, 444-451.

Udeshi, N.D., Svinkina, T., Mertins, P., Kuhn, E., Mani, D.R., Qiao, J.W., Carr, S.A. (2013). Refined preparation and use of anti-diglycine remnant (K-epsilon-GG) antibody enables routine quantification of 10,000s of ubiquitination sites in single proteomics experiments. Molecular & Cellular Proteomics 12, 825-831.

Vitale, C.L., Olby, N.J. (2007). Neurologic dysfunction in hypothyroid, hyperlipidemic Labrador Retrievers. J Vet Intern Med 21(6), 1316-1322.

Wang, G.D., Zhai, W., Yang, H.C., Fan, R.X., Cao, X., Zhong, L., Wang, L., Liu, F., Wu, H., Cheng, L.G., et al. (2013). The genomics of selection in dogs

and the parallel evolution between dogs and humans. Nat Commun 4, 1860.

Wang, T., Ma, J., Hogan, A.N., Fong, S., Licon, K., Tsui, B., Kreisberg, J.F., Adams, P.D., Carvunis, A.R., Bannasch, D.L., et al. (2020). Quantitative Translation of Dog-to-Human Aging by Conserved Remodeling of the DNA Methylome. Cell Syst 11, 176-185 e176.

Weiss, D., Kools, J.J., Taylor, W.R. (2001). Angiotensin II-induced hypertension accelerates the development of atherosclerosis in apoE-deficient mice. Circulation 103(3), 448-454.

Yin, W., Carballo-Jane, E., McLaren, D.G., Mendoza, V.H., Gagen, K., Geoghagen, N.S., McNamara, L.A., Gorski, J.N., Eiermann, G.J., Petrov, A., et al. (2012). Plasma lipid profiling across species for the identification of optimal animal models of human dyslipidemia. J Lipid Res 53(1), 51-65.

Zhang, S.H., Reddick, R.L., Piedrahita, J.A., Maeda, N. (1992). Spontaneous hypercholesterolemia and arterial lesions in mice lacking apolipoprotein E. Science 258, 468-471.

Zhao, Y., Yang, Y., Xing, R., Cui, X., Xiao, Y., Xie, L., You, P., Wang, T., Zeng, L., Peng, W., et al. (2018). Hyperlipidemia induces typical atherosclerosis development in Ldlr and Apoe deficient rats. Atherosclerosis 271, 26-35.

Compliance and ethics

We declare that we have no conflict of interest.

Acknowledgements:

We thank Drs Jie Du, Xun Huang, Si Cheng, Wei Li, and Yi Ding for discussion, and John Speakman for critical reading of an early version of the manuscript.

Funding

Xunming Ji is supported by the National Natural Science Foundation of China (NSFC; grant number 81620108011) and the Ministry of Science and Technology of China (MOST; 2017YFC1308401). Yong Q. Zhang is supported by NSFC (31830036 and 31921002), the Beijing Municipal Science & Technology Commission (Z181100001518001), MOST (2019YFA0707100), and the Chinese Academy of Sciences (XDBS1020100).

Author Contributions

XJ and YZ conceptualized the project, supervised data collection and analysis. HZ, JZ, DW, and ZS designed the research experiments and performed the majority of experiments. YH, MZ, Yumei L, and QY performed brain imaging and ultrasonography examination. XH, Ying W, and ZD performed proteomic analysis. YP, and HX performed immunostaining analysis. Yuan L and HY performed surgery. SL and GS performed lipidomic analysis. HZ, ZS, and YZ wrote the manuscript, and Yongjun W, LL, EL and JM provided advice and commented on the manuscript.

Abbreviations

ADC: apparent diffusion coefficient

ApoE: Apolipoprotein E

CCA: common carotid artery

CRISPR: clustered regularly interspaced short palindromic repeats

DWI: diffusion weighted imaging

ECA: external carotid artery

ECG: electrocardiography

EDV: end diastolic velocity

FLAIR: fluid attenuated inversion recovery

GWAS: genome-wide association study

. HDL-C: high-density lipoprotein cholesterol

. . ICA: internal carotid artery

. / IDL: intermediate-density lipoprotein

. 0 KO: knockout

. LDL: low-density lipoprotein

. LDL-C: low-density lipoprotein cholesterol

. MRI: Magnetic Resonance Imaging

. PSV: peak systolic velocity

. SDS-PAGE: sodium dodecyl sulfate-polyacrylamide gel electrophoresis

. SMA: smooth muscle actin

. T2W: T2-weighted

. . TC: total cholesterol

. / VLDL: very low-density lipoprotein

. 0 WT: wild type

. .

Figure Legends

Figure 1

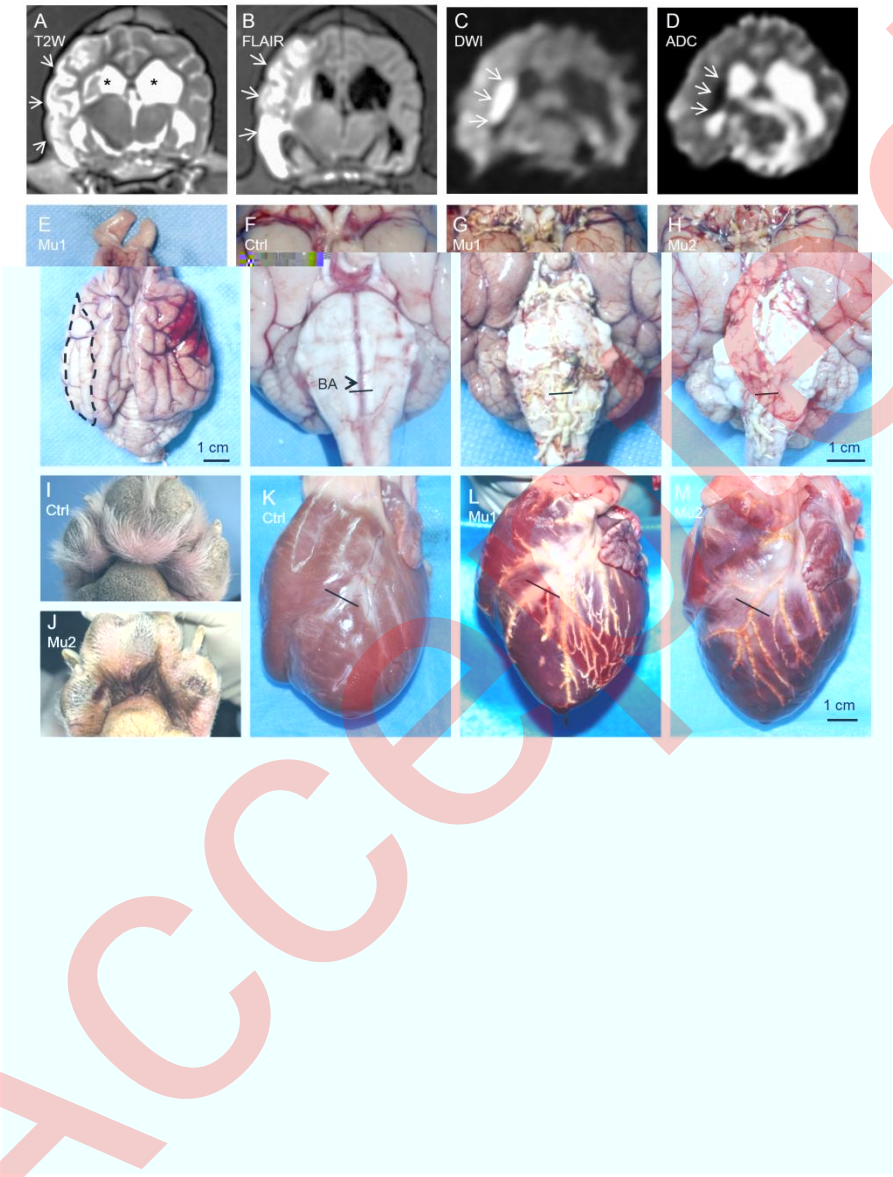

Figure 1. Brain MRI and sclerotic arteries of the brain and heart in *ApoE* KO dogs

A, T2 weighted (T2W); B, fluid attenuated inversion recovery (FLAIR); C, diffusion weighted imaging (DWI), and D, apparent diffusion coefficient (ADC) brain images for *ApoE* mutant 1. Arrows in A and B point at a large infarct of 7.41 cm^3 in left frontal, parietal, and temporal lobe, while arrows in C and D indicate a later, small ischemic infarct of 1.14 cm^3 in the left basal ganglia.

. / Asterisks indicate ventricles of different sizes. E, There was subarachnoid
. / hemorrhage with an unknown reason on the surface of right brain (E)
. / compared with the normal control. An infarct in the left brain of mutant 1 is
. / delineated by dashed lines (E). F, G and H, The intracranial basilar arteries
. / (BA) of *ApoE* mutant 1 (G) and 2 (H) appear bulged and yellowish compared
. / with the WT control (F). Scale bar, 1 cm. I and J, *ApoE* KO mutant 2 developed
. / gangrene in the left hind paw (J) compared with the normal control (I). K, L and
. / . M, Compared with WT (K), the coronary arteries in *ApoE* mutant 1 (L) and 2 (M)
. / / are unevenly bulged and yellowish, indicative of atherosclerosis. Scale bar, 1
. / 0 cm. Red lines indicate positions for pathological analysis.

Figure 2

. 0

. 0 **Figure 2. Ultrasonography examination of plaques and occlusion in the**

. 0 **internal carotids of *ApoE* KO dogs**

. 0 A and C, The right (A) and left (C) common carotid artery (CCA) and internal

. 0 carotid artery (ICA) of the *ApoE* mutant 1, examined by the B mode

. 0 ultrasonography. The plaques are 6.5 x 1.2 mm in the right and 4.1 x 1.2 mm in

. 0 the left ICA. The inset in A shows a plaque (denoted by a red asterisk) from

. 0. another perspective. A white arrow in C points at an occlusion in the left ICA. B

. 0/ and D, Blood flow velocity was at 24 cm/s peak systolic velocity (PSV)/6 cm/s

. 00 end diastolic velocity (EDV) in the less affected right ICA (B) but a more
/ reduced blood flow was observed in the more severely affected left ICA (D)
/ with a flow velocity at 21 cm/s (PSV)/-5.6 cm/s (EDV) at the proximal ICA for
/ the mutant 1 detected by spectral Doppler mode ultrasonography. E and G,
/ The right (E) and left (G) CCA, external carotid artery (ECA), and ICA of the
/ normal control dog examined by B mode ultrasonography. The diameter of the
/ proximal ICA was 1.8 mm for the right ICA (E) and 2.1 mm for the left ICA (G)
/ (indicated by two small crosses). F and H, The blood vessel had a flow velocity
/ . at 40.5 cm/s (PSV)/12.4 cm/s (EDV) for the right ICA (F) and 32.6 cm/s
/ / (PSV)/12.0 cm/s (EDV) for the left ICA (H) examined by spectral Doppler mode
/ 0 ultrasonography.

Figure 3

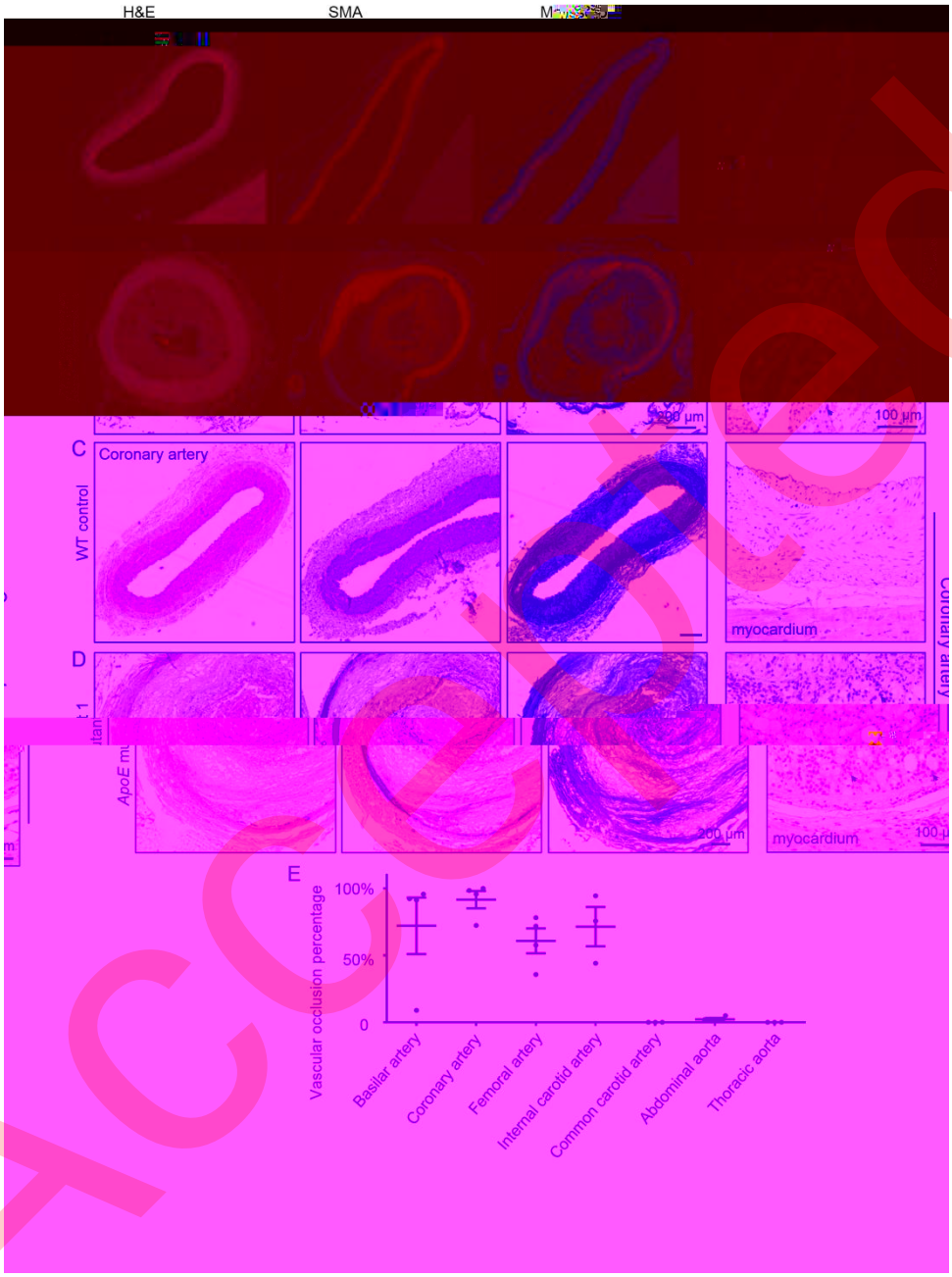

/

/ **Figure 3. Severe atherosclerosis revealed by histological staining of**

/ **basilar and coronary arteries in *ApoE* null mutants.**

/ A–D, Histological staining of the basilar artery and the paraconal

/ interventricular branch of the left coronary artery of 2-year-old normal control

/ (A, C) and *ApoE* mutant 1 (B, D). Cross sections of basilar artery and coronary

/ artery stained with H&E, anti-SMA, and Masson of WT control and *ApoE*

/ . mutant 1. Anti-SMA stains smooth muscles. Masson staining marks muscle
/ / fibers (red) and collagen fibers (blue) in the artery. CD68 labels macrophages
/ 0 (brown, positive cells pointed by arrowheads). Substantial thickening of the
/ tunica intima layer filled with foam cells is apparent in the basilar artery (B).
/ Severe or complete occlusion of vessels by plaques are apparent in the
/ mutant arteries (B and D compared with A and C, respectively). Scale bar, 200
/ μm in columns 1, 2, 3 and 100 μm in column 4. E, Quantitative analysis of
/ atherosclerosis in different arteries by the percentage of increased intimal area
/ filling up the vascular lumen. n = 4 in mutants. The values in WT controls (n = 4)
/ are all 0.

Figure 4

Figure 4. Immunostaining reveals severe atherosclerosis in the internal carotid artery of the *ApoE* KO dogs.

A–C, H&E staining of the proximal internal carotid of a 2-year-old WT control (A) and *ApoE* mutant 1 (B) and mutant 2 (C). D–I, Cross sections of internal carotid stained with anti-SMA (D to F), Masson (G to I) of WT control (D and G) and *ApoE* mutant 1 (E and H) and 2 (F and I). Tunica intima (a thin layer of teeth-like structures denoted by an arrow), tunica media, and tunica adventitia

of the vessels are indicated in D. An occlusive luminal thrombus (TH, in B and H) consisting of red blood cells and cholesterol crystals (indicated by an asterisk in B) was observed in the internal carotid of *ApoE* mutant 1 (B, E and H). An arrow in F indicates detached tunica intima close to rupture. Fibrous tissue (F) and fully developed necrotic cores (NC) are denoted in the internal carotid of mutant 2 (F).

Figure 5

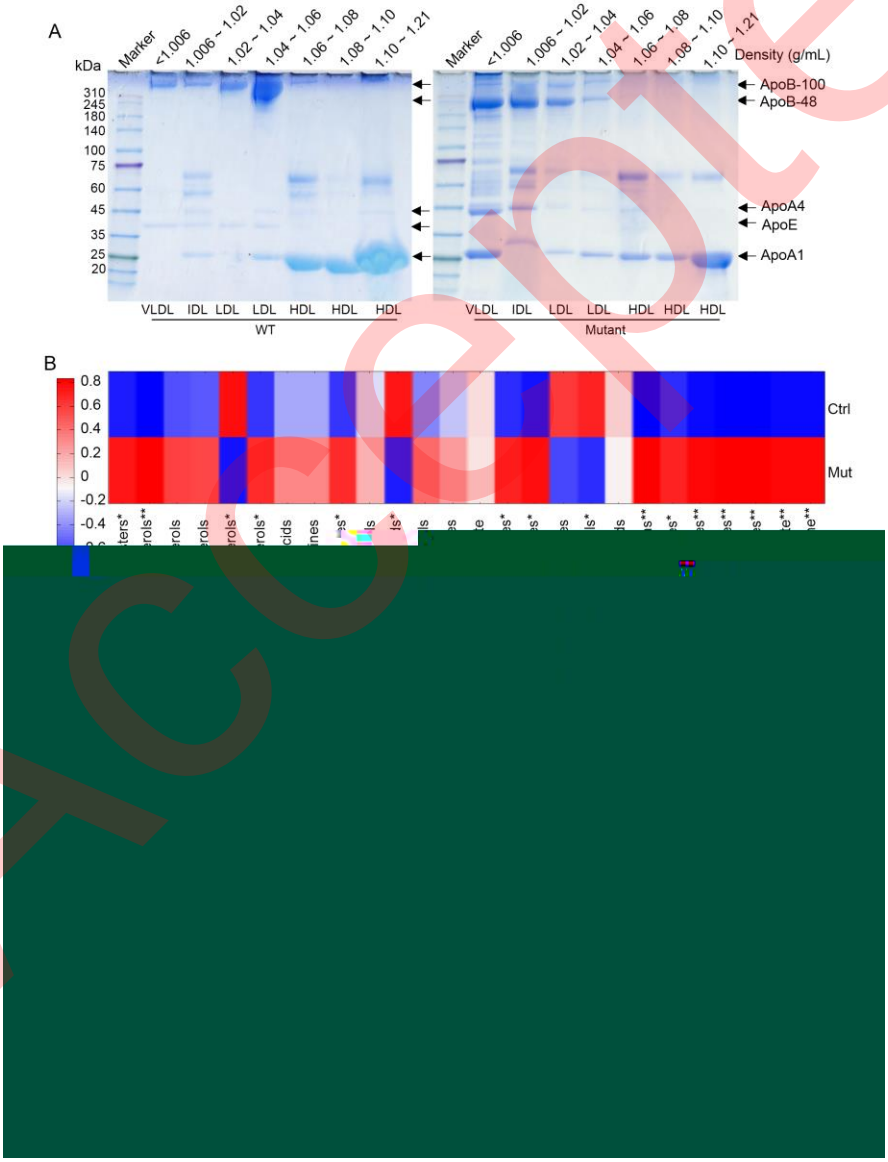

Figure 5, Analysis of lipoproteins and lipid composition in the plasma of *ApoE* mutant dogs.

/ A, SDS-PAGE analysis of lipoproteins in the plasma fractionations by
/ sequential ultracentrifugation from WT control and *ApoE* mutant dogs.
/ Different fractionations of plasma of WT and F2 homozygous *ApoE* mutant
/ . dogs (40 μL for each fractions) were resolved by 4-20% SDS-PAGE, followed
/ / by Coomassie brilliant blue staining. *ApoE* KO dogs showed absence of ApoE
/ 0 and a marked increase of ApoB-48, ApoA4 and ApoA1 in the VLDL fraction
/ compared with WT controls. B, Heat map showing the levels of different lipid
/ components in the plasma of WT and *ApoE* KO dogs. n = 4 in each group. *P <
/ 0.05, ** P < 0.01 by student's *t* test.

.

Figure 6

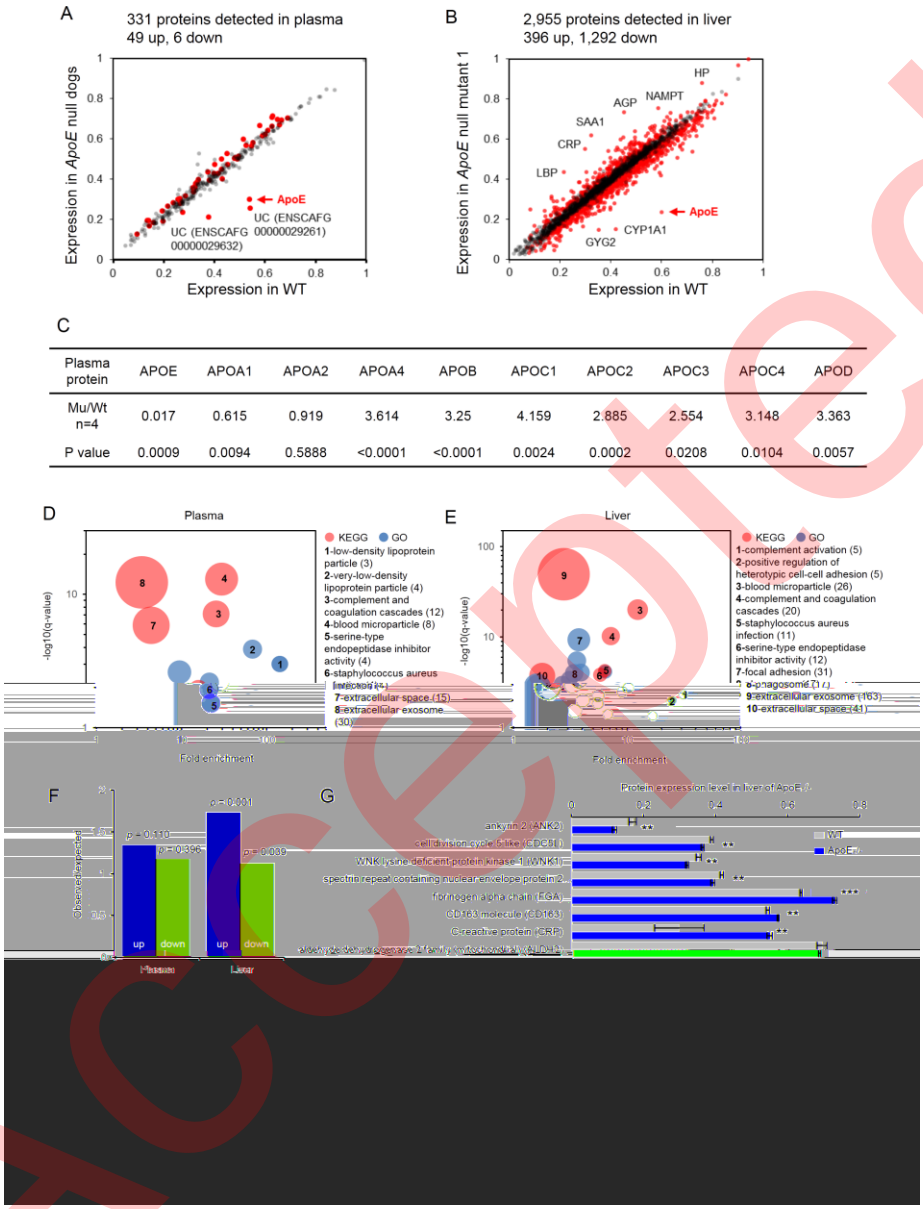

Plasma protein	APOE	APOA1	APOA2	APOA4	APOB	APOC1	APOC2	APOC3	APOC4	APOD
Mu/Wt n=4	0.017	0.615	0.919	3.614	3.25	4.159	2.885	2.554	3.148	3.363
P value	0.0009	0.0094	0.5888	<0.0001	<0.0001	0.0024	0.0002	0.0208	0.0104	0.0057

/

/ **Figure 6. Proteomic analyses reveal altered lipoprotein and**
/ **stroke-related protein levels in the *ApoE* KO dogs.**

/ A and B, Proteomic analyses detected proteins in the plasma (A) and liver (B)
/ . of *ApoE* KO dogs and WT controls. Proteins with significant expression level
/ / changes are shown in red. The arrows highlight the reduced expression of
/ 0 ApoE protein in mutants. C, A list of altered lipoprotein levels including ApoE in
/ plasma (n = 4 for both mutants and controls). D and E, Bubble plots showing
/ fold enrichment and -log10 q-values (Benjamini-Hochberg corrected *P* value)

/

/ of all enriched functional terms for upregulated proteins in plasma (D) and liver
/ (E) of *ApoE* KOs. Red bubble indicates KEGG pathway, and blue indicates
/ Gene Ontology analysis. Bubble size corresponds to the number of genes
/ changed for the functional term. F, Fold enrichment in canine homologs of
/ human stroke related genes. The bar graph shows the ratio of observed to
/ . expected numbers of stroke related genes in up- (red) and down-regulated
/ / (blue) proteins in plasma and liver of *ApoE* KOs. G, A comparison of protein
/ 0 levels of canine homologs of human GWAS-positive stroke genes in the liver
/ . from the WT and *ApoE* mutant 1.

/ .

/ . GGFI @ @ FI 8 @

/ . 1 . .

/ .

/ .

/ .

/ . .

Table 1

Atherosclerotic lesions in F0 *ApoE* dogs at 18–24 month old detected by ultrasonography

Artery		Mutant 1 24 months	Mutant 2 18 months	Mutant 3 18 months	Mutant 4 18 months
Carotid artery	Left internal	occlusion	stenosis	plaque	plaque
	Left external	thickened	stenosis	thickened	plaque
	Left common	thickened	plaque	plaque	NA
	Right internal	stenosis	stenosis	thickened	NA
	Right external	thickened	stenosis	thickened	plaque
	Right common	thickened	plaque	thickened	NA
Abdominal aorta	Top	plaque	thickened	thickened	thickened
	Middle	thickened	plaque	thickened	thickened
	Lower	thickened	plaque	thickened	thickened
Femoral artery	Left common	thickened	thickened	thickened	thickened
	Left superficial	plaque	thickened	thickened	NA
	Left deep	thickened	thickened	thickened	NA
	Right common	thickened	thickened	thickened	thickened
	Right superficial	plaque	thickened	thickened	NA
	Right deep	thickened	thickened	thickened	NA

Thickened denotes thickened walls of blood vessels. The severity of atherosclerosis from weak to strong is thickened, plaque, stenosis, and occlusion as described in Materials and Methods section. NA, not available.

/ / **Table 2**

/ / Atherosclerotic lesions in F2 homozygous *ApoE* dogs at 9–17 month old
/ / . detected by ultrasonography

Artery		-2236/ -2236 bp 17 months	-34+17/ -34+17 bp 17 months	-34+17/ -34+17 bp 12 months	-34+17/ -34+17 bp 9 months
Carotid artery	Left internal	stenosis	normal	normal	normal
	Left external	plaque	normal	normal	normal
	Left common	thickened	normal	normal	normal
	Right internal	plaque	normal	normal	plaque
	Right external	stenosis	normal	normal	thickened
	Right common	thickened	normal	normal	plaque
Abdominal aorta	Top	thickened	normal	normal	normal
	Middle	thickened	normal	normal	normal
	Lower	thickened	normal	normal	normal
Femoral artery	Left common	stenosis	normal	thickened	normal
	Left superficial	plaque	normal	thickened	normal
	Left deep	plaque	normal	thickened	normal
	Right common	stenosis	thickened	normal	normal
	Right superficial	plaque	thickened	normal	normal
	Right deep	plaque	thickened	normal	normal

/ / / Thickened denotes thickened walls of blood vessels. The severity of atherosclerosis from

/ / 0 weak to strong is thickened, plaque, stenosis, and occlusion as described in Materials and

/ 0 Methods.

/ 0

Table 3

Increased cholesterol level in the plasma of *ApoE* KO dogs before weaning

Plasma lipids	WT control +/+ (*n* = 27)	F2 -/- (*n* = 4)	F3 -/- (*n* = 9)
TC (mmol/L)	4.57±0.24	24.83±2.11***	20.23±2.09***
TG (mmol/L)	0.90±0.06	0.87±0.25	1.20±0.20
LDL-C (mmol/L)	0.54±0.06	15.80±1.59***	12.7±1.52***
HDL-C (mmol/L)	3.33±0.20	4.66±0.28	3.73±0.15

F2, F3 mutant dogs and wild type controls were analyzed at 1–2 months old. Blood was drawn from the limb venous plexus into EDTA tubes after 14 hours starvation. TC, total cholesterol; TG, triglycerides; LDL-C, low density lipoprotein cholesterol; HDL-C, high density lipoprotein cholesterol. Data are presented Mean ± SEM. -/-, homozygous; +/-, heterozygous; +/+, WT. *P < 0.05, **P < 0.01, ***P < 0.001, as determined by One way ANOVA and Dunnett's multiple comparisons tests for mutants vs. WT control.

Table 4

Increased level of total cholesterol in the plasma of adult *ApoE* KO dogs

Plasma lipids	F0		F2	
	-/- (*n* = 4)	+/+ (*n* = 10)	-/- (*n* = 4)	+/+ (*n* = 10)
TC (mmol/L)	24.94±2.2***	4.03±0.2	25.44±4.92***	4.92±0.30
TG (mmol/L)	0.417±0.03	0.40±0.02	1.35±0.84	0.51±0.05
LDL-C (mmol/L)	19.39±2.1***	0.4±0.08	17.47±4.11***	0.55±0.12
HDL-C (mmol/L)	2.46±0.28**	3.81±0.15	3.22±0.39	4.06±0.26

F0 mutant dogs and controls were analyzed at 18–24 months old. F2 mutant dogs and controls were analyzed at 7–17 months old. Blood was drawn from the limb venous plexus into EDTA tubes after 14 hours starvation. TC, total cholesterol; TG, triglycerides; LDL-C, low density lipoprotein cholesterol; HDL-C, high density lipoprotein cholesterol; Data are presented Mean ± SEM. -/-, homozygous; +/+, WT. ***P* < 0.01, ****P* < 0.001, as determined by a two-tailed Student's *t* test for both F0 mutants and F2 mutants.